

# High-Efficient Solar Cell Design Using Green Synthesized ZnO From Gundruk Using a Numerical Approach

Sagar Bhattarai\*

Department of Physics, Arunachal University of Studies,  
Namsai, Arunachal Pradesh, 791112, India

**\*Correspondence author**

**Sagar Bhattarai,**  
Department of Physics  
Arunachal University of Studies  
Namsai  
Arunachal Pradesh  
India

Submitted : 10 Mar 2023 ; Published : 29 Apr 2023

**Citation :** Bhattarai S., High-Efficient Solar Cell Design Using Green Synthesized ZnO From Gundruk Using a Numerical Approach. *J mate poly sci*, 3(2): 1-6.

## Abstract

In this paper, we observe a comprehensive simulation approach for organic/inorganic perovskite absorber layer (PAL)-based photovoltaic solar cell under the preconditioned illumination of AM1.5 for distinct device structures. The predominant objective of this work is to investigate the optimization of thickness parameters of the lead-free PAL active layer attached to the device structures to attain the best possible efficiency for the lead-free PAL, i.e.,  $\text{MASnI}_3$ -based PSC. The present simulation accomplishes considering green synthesized ZnO as an electron transport layer (ETL) and P3HT as a hole transport layer (HTL), sandwiching the PAL layer of  $\text{MASnI}_3$  having a precise bandgap of 1.3 eV. Therefore, the extensive investigation of the simulated device structures confirms the optimized thickness of the ETL,  $\text{MASnI}_3$ , and HTL, respectively, as 100 nm, 600 nm, and 100 nm for the device structure. Optimizing layer thickness using green synthesized ZnO yields a much-improved power conversion efficiency (PCE) approaching 22% owing to enhanced  $J_{sc}$ , enriching the earlier reported value of Bhattarai et al. (2022) PSC devices.

**Keywords:** perovskite absorber layer (PAL),  $\text{MASnI}_3$ , electron transport layer (ETL), power conversion efficiency (PCE).

## Introduction

The perovskite-structured organometallic halides with a compositional structure of  $\text{ABX}_3$  have played a sensational role in revolutionizing the field related to organic-inorganic hybrid solar cells. As the archetypical structure of  $\text{ABX}_3$  (Abdelaziz et al., 2022; Bhattarai et al., 2022; Bhattarai et al., 2021; Cha et al., 2016; Bhattarai et al., 2023) comprises of A, which is a methylammonium cation ( $\text{MA}^+$ ) comparatively larger ionic radius of 0.18 nm than B and X ions, and the cation B usually considered as Pb or Sn, and X is halide material (Lakhdar & Hima, 2020; Pandey et al., 2021). Since the previous decade, the PSC has emerged as a better alternative due to its excellent optoelectronic properties, such as strong visible range absorption, accreditation with longer charge carrier diffusion lengths and improved efficiency (Raoui et al., 2021; Rahman et al., n.a.; Bhattarai et al., 2020; Ahmmed et al., 2021; Bhattarai et al., 2022). The development of the PSC structure was initiated with the pioneered work by Kojima et al. at which the active layer was constructed with  $\text{CH}_3\text{NH}_3\text{PbX}_3$ , where PCE up to 3.8% was reported using Br as the halide materials (Kojima et al., 2009). Carrying forward, the numerous research for improving its efficiencies in PSC devices was exponentially grown-up until the current scenario. While the better selection of related materials with optimized thickness in the PSC layer

structures is mandatory for the optimization of the device efficiency. In this sequence, considering 2,20,7,70-tetrakis-(N, N- di-p-methoxyphenylamine)-9,90-spiro-biurene (Spiro-OMeTAD) as a solid-state hole transfer material (HTL) enhancing the PCE nearly to 10% by Kim et al. (2016). The simple and easy fabrication attribution made these types of planer heterojunction perovskite solar cells an effective alternative to the mesoscopic design. However, the major problem in the PSC device fabrication is obtaining the best optoelectronic parameters through the thickness optimization of the light-harvesting Layer as it impacts the cellular output. Since, the thinner active Layer in PSC results in lower photon absorption, further contributing to attaining lower photocurrent density. While the thicker perovskite active Layer results in lower charge extraction and the recombination becomes very challenging in the PSC device in the range of 100 nm to 400 nm (Bhattarai et al., 2020). So, attaining the suitable thickness with a doping concentration of acceptor and donor for the constituent layers in PSC is the finest and most effective approach for finding more cellular output in the PSC devices. Although the significant progress in lead-based PAL material in the recent decade has extended much attention, the toxicity of the lead material remains the major hindrance to the wider

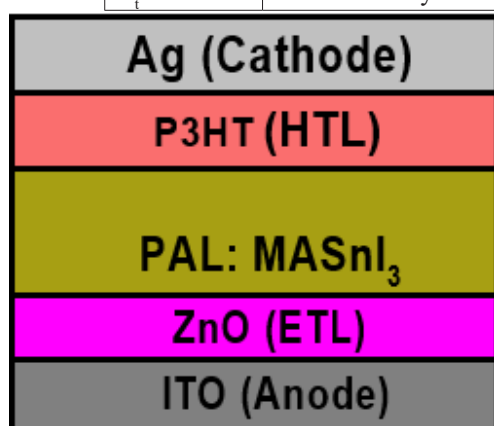
application of the PSC. To sort out the problem, lead (Pb) can be replaced with tin (Sn) in the PAL layer, as previous reports also confirmed the Bandgap of the MASnI<sub>3</sub> based PAL layer is nearly 1.3 eV, which is much lesser than the methylammonium lead iodide (MALI) (~1.6 eV) based PAL layer (Bhattarai et al., 2021). As the lesser Bandgap for MASnI<sub>3</sub> will absorb photons with a much wider visible range than MALI. In this paper, we used the solar irradiance of 1.5AM as the input of light source for the calculation of the optical profile, which can be transferred to an electrical model for evaluation of carrier transport phenomena and electronic output at different vacuum level bandgap for MASnI<sub>3</sub>-based PSC by the simulation study under the doping concentration of the acceptor and the donor. Using a commercially available software package, the study also investigated the capacitance-voltage (C-V) parameters for both device structures. The basic solar cell parameters like short circuit current density ( $J_{sc}$ ), open-circuit voltage ( $V_{oc}$ ), fill factor (FF) and power conversion efficiency (PCE) is also investigated for the proposed MASnI<sub>3</sub>-based PSC structure at the different thickness of the ETL, PAL, and HTL respectively.

### Simulated Device Structure

A heterojunction perovskite solar cell with n-i-p configuration ITO/ZnO (green synthesized)/ MASnI<sub>3</sub> /P3HT/Ag is considered for the simulation of the PSC device as shown in Figure.1(a). The typical PSC device is constructed with ITO as a top electrode having a thickness of 100 nm followed by a green synthesized ZnO (biosynthesized from radish roots, i.e. Gundruk ; famous food from radish by Gorkha community) of 100 nm which functions as an ETL i.e. electron Transporting Layer, effectively collects photogenerated electrons from PAL in the PSC device structure. The PAL materials for the devices have a precise thickness of 400 nm as it's sandwiched between both the ETL and HTL. As the thickness of 100 nm of P3HT effectively collects the hole from the PAL and transfers it to the anode through the hooping mechanism. The cathode is considered Ag, containing a thickness range of 100 nm. However, the energy mismatch in the intermediate organic Layer triggers the flowing of the electron from the higher energy state to the lower energy state i.e. from right to left as shown in Figure 1(b). As the photogenerated electron in PAL primarily inject to ETL and hole to HTL and is further collected by their respective electrodes (Bhattarai et al., 2021).

**Table 1:** The input parameters in the simulating devices, where d (nm) is the Thickness,  $E_g$  (eV) is the Bandgap,  $\epsilon_r$  is Relative Permittivity,  $N_c$ (cm<sup>-3</sup>) is Effective DoS at CB,  $N_v$ (cm<sup>-3</sup>) is the Effective DoS at VB,  $\mu_n$ (cm<sup>2</sup>/Vs) is the Mobility of electrons,  $\mu_p$ (cm<sup>2</sup>/Vs) is the Mobility of holes,  $D_a$ (m<sup>-3</sup>) is the Doping conc. of the acceptor,  $D_d$ (m<sup>-3</sup>) is the Doping conc. of donor, and  $N_t$  is Defect Density (Bhattarai et al., 2022; Madan et al., 2020; Bhattarai & Das, 2021).

Parameter	Terms	ETM (ZnO from Gundruk)	PAL (MASnI <sub>3</sub> )	HTM (P3HT)
d (nm)	Thickness	100	600	100
$E_g$ (eV)	Bandgap	3.5	1.3	3.1
	Relative Permittivity	9	8.2	3.4
$N_c$ (cm <sup>-3</sup> )	Effective DoS at CB	$2.2 \times 10^{17}$	$2 \times 10^{18}$	$1 \times 10^{22}$
$N_v$ (cm <sup>-3</sup> )	Effective DoS at VB	$2.2 \times 10^{16}$	$2 \times 10^{18}$	$1 \times 10^{22}$
$\mu_n$ (cm <sup>2</sup> /Vs)	Mobility of electrons	20	1.6	$1 \times 10^{-4}$
$\mu_p$ (cm <sup>2</sup> /Vs)	Mobility of holes	10	1.6	$1 \times 10^{-3}$
$D_a$ (cm <sup>-3</sup> )	Doping conc. of the acceptor	0	0	$1 \times 10^{18}$
$D_d$ (cm <sup>-3</sup> )	Doping conc. of donor	$1 \times 10^{17}$	$1 \times 10^{19}$	0
$N_t$	Defect Density	$1 \times 10^{14}$	$1 \times 10^{14}$	$1 \times 10^{14}$



(a)

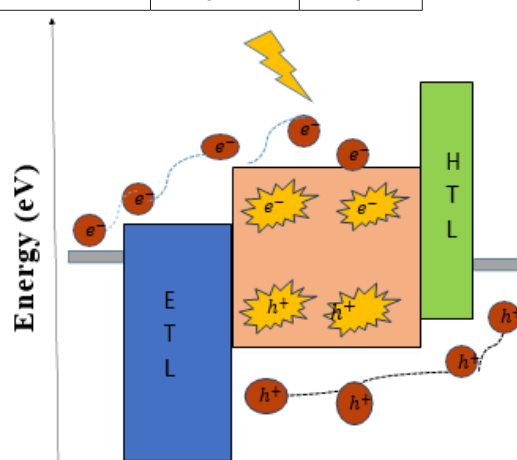


**Figure 1:** (a) Schematics layers of the simulated PSC devices and (b) the working mechanism of the devices under the illuminance of AM1.5.

## Results And Discussions

### Comparison of perovskite thicknesses of both the PSC devices

The simulation study has been undertaken with the designated extension of the parameters in the preconditioned doping density as listed in table 1 at a room temperature of 300K. In Figure. 2, the effect of PAL layer thickness on the electric parameters for the device structures namely has been demonstrated. It can be well observed in Figure. 2(a), that the short circuit current density ( $J_{sc}$ ) for both the devices increases with increasing the PAL layer thickness up to a saturated value of 32.20 mA/cm<sup>2</sup>, at 600 nm. This can be explained more collectively as the PAL thickness of 600 nm enhances the rate of excitons generation due to more absorbance in the small Bandgap of PAL layers, i.e. 1.3eV. Therefore, the electron mobility in the active Layer is effectively triggered due to the higher excitons generation in the devices. Figure. 2(b) represents the variation of  $V_{oc}$  over

the PAL layer thicknesses ranging from 200 nm to 800 nm. A non- monotonic change of  $V_{oc}$  up to 400 nm thickness remains in steady-state as most of the photon is absorbed by this precise thickness in the active Layer in the PSC. However, in Figure. 2(c), FF is decreasing from 200 nm to 800 nm range. The PCE variation for both perovskite devices with the function of the active layer thickness is shown in Figure. 2(d), as the PSC device enriching highest PCE corresponding to a thickness 600 nm. The PCE for the PSC is collectively improved from 18.48% to a maximal value of 22.01%. The device offers much higher  $J_{sc}$  for a smaller bandgap in the PAL layer, which absorbs photons of much wider frequencies (Karthick et al., 2020). The simulated device has achieved highly improved solar cell parameters than Adhikari et al. (2016). As the considerable increase in  $J_{sc}$  for the active layer thickness of 600 nm is due to the higher generation of the excitons pairs, which extensively affect the PCE of the PSC devices.

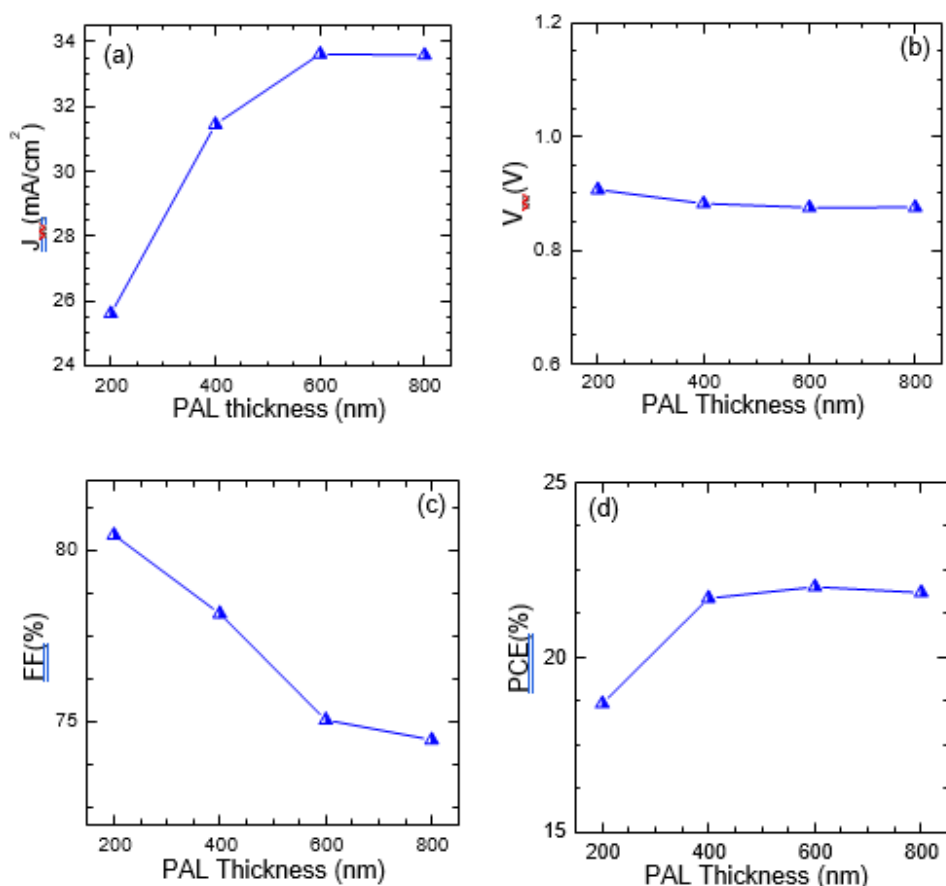


**Figure 2:** Perovskite solar cell outputs over the different thickness of active layers

### Impact of the temperature on the PSC devices

The complete analysis of solar cell properties with temperature fluctuation is shown in Figure 3. The final parameters, i.e. PCE drop as the temperature increases from 300 K to 400 K, as seen in the graph below. The degradation of the materials caused by the temperature increase from 300 K to 400 K is what caused the parameters to decline. Due to the continuous degrade of the  $V_{oc}$  that exhibits the highest values at 300K, i.e. 22.01% and the lowest value at 400 K, i.e, 14.05%, respectively. Similarly, trends can be seen in the previous works by Bhattarai et al. (2022).

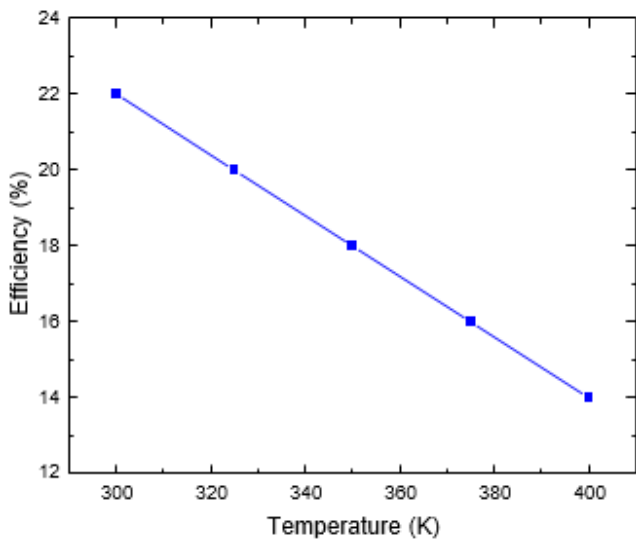


**Figure 3:** Impact of the temperature on the efficiency of the PSC.

**Impact of the total defect density on the PSC devices**

The defect density analysis is one of the most appropriate methods for improving the efficiency of PSC devices. The defectivity of the simulated MASnI<sub>3</sub> varied from 1×10<sup>14</sup> cm<sup>-3</sup> to 1×10<sup>18</sup> cm<sup>-3</sup>, as depicted in Figure. 4. Firstly, the device offers a high efficiency of 22.01%, whereas it keeps decreasing up to 13.34% by increasing the defect density to 1×10<sup>18</sup> cm<sup>-3</sup>. The pi chart described how many fractions of efficiency is obtained for both the PSC devices. As the change of fractions with the defects can be obtained from the pi-chart as depicted below. Further, the overall outputs of the solar cell parameters has been listed in Table 2. The formation of incomplete dangling bonds occurs during the material synthesis when experimentally fabricating the device. These dangling bonds result in additional defect levels within the material’s bandgap, act as a recombination center, and affect the carrier lifetime and diffusion length. Therefore, to account for defect-related recombination/carrier lifetime/diffusion length, we considered bulk defect density inside the material to perform a realistic device simulation. Considered defect density is listed in Table 1.

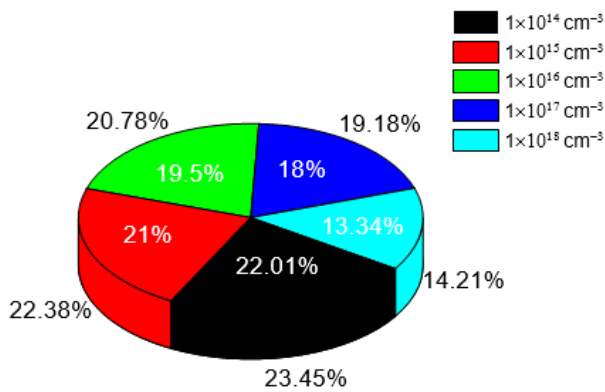


**Figure 4:** Impact of the total defect density on the efficiency of the PSC.

**Impact of different cathodes on different outputs**

The charge carrier is captured at the solar cell’s two opposing ends depends on the type of metal contact. Whether the contact is Schottky or ohmic, it depends. The Schottky creates an energy barrier that prevents the bulk of charge carriers from leaving the device. The ohmic contact, on the other hand, enables a simple flow of such carriers. The expense of producing such a device is increased by the use of pricey contact materials like Au. As contact materials for HTL, we have used Cu, Ag, C, Pt, and Au in all three of the devices discussed in this study. The conversion efficiency of the devices with various back contact materials is shown in Figure.5. Remarkably, in the PSC devices, C and Ag with large work functions (>5 eV) perform the best. Therefore, verifying that those materials made an ohmic contact with the HTL layer is possible.

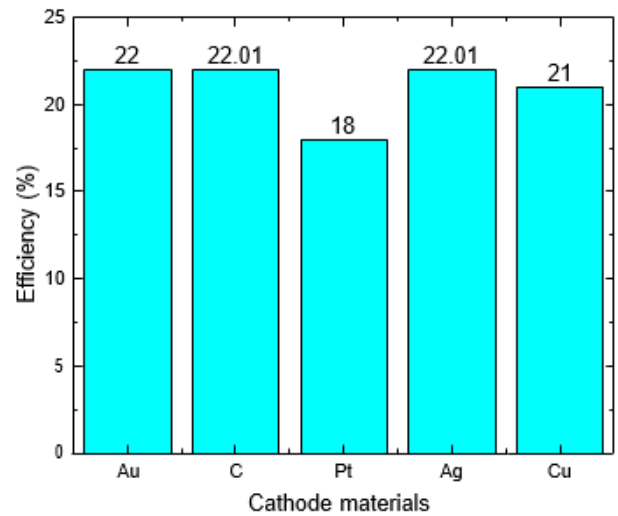


**Figure 5:** Impact of the cathode materials on the efficiency of the PSC.

**The J-V characteristics of both the PSC optimized conditions**

The J-V parameter for PSC devices with the optimized thickness and temperature of 800 nm and 300 K is depicted as shown in Figure 6. Firstly, in, the current density increases with the increase in the thickness and reaches a saturated value at the thickness level of 0.8 μm. This may be due to extensive higher absorption in the higher thickness level. While in, increasing the defects greatly impacts the voltages and lowers the voltage as it achieves a value of 1.6 V at a higher defect density value. The high V<sub>oc</sub> for the PSC device offers a much better PCE as shown in table 2. The present work is much improved than the previous work of Rai et al. (2020).

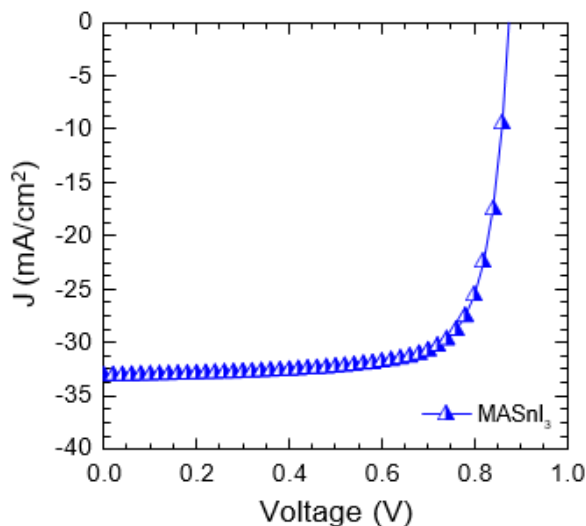


**Figure 6:** The J-V of the Perovskite solar cell device structure at optimized conditions.

**Table 2:** Simulated PV device characteristics along with earlier works.

Device structure	$J_{sc}$ (mA/cm <sup>2</sup> )	$V_{oc}$ (V)	FF (%)	PCE (%)
MASnI <sub>3</sub> based PSC	33.62	0.875	75.94	22.01
Bhattacharai et al. [1]	33.19	0.876	76.19	22.16

### Conclusion

In summary, we study the predominant solar cell parameters using the charge carrier transport phenomena for lead-free PAL layers under green synthesized ZnO materials. It can be well predicted that the PSC device structure's PAL layer significantly impacts the electric parameter more than the carrier transport layers (ETLs and HTLs). Therefore, we obtain the optimized PSC parameters at the thickness level of 800 nm, 100 nm, and 100 nm for PAL, ETL, and HTL, respectively. Specifically, the PSC offers a high  $J_{sc}$  of 33.62 mA/cm<sup>2</sup>,  $V_{oc}$  of 0.875 Volt, FF of about 76%, and PCE of 22.01%. The green-synthesized ZnO offers a similar impact as compared to the conventional ZnO materials. The PCE reported matches the previously reported value of Bhattacharai[1] et al.. Thus, the study provides an impactful guideline and has proven to be helpful in enhancing its efficiency with the reasonable fabrication of MASnI<sub>3</sub>-based PSC devices.

### Acknowledgment

The authors acknowledge the SCAPS-1D development team for providing the simulator for our research work.

### References

1. Bhattacharai, S., Pandey, R., Madan, J., Mhamdi, A., Bouazizi, A., Muchahary, D., Gogoi, D., Sharma, A. & Das, T. D. (2022). "Investigation of Carrier Transport Materials for Performance Assessment of Lead-Free Perovskite Solar Cells," *IEEE Transactions on Electron Devices*, 69, no. 6, pp. 3217-3224.

2. Abdelaziz, S., Zekry, A., Shaker, A., & Abouelatta, M. (2022). "Investigating the performance of formamidinium tin-based perovskite solar cell by SCAPS device simulation," *Optical Materials*, 101, pp. 109738.
3. Bhattacharai, S., Pandey, R., Madan, J., Ahmed, F. & Shabnam, S. (2022). "Performance improvement approach of all inorganic perovskite solar cell with numerical simulation," *Materials Today Communications*, 33, pp. 104364.
4. Bhattacharai, S., Sharma, A., Swain, P. K., & Das, T. D. (2021). "Numerical Simulation to Design an Efficient Perovskite Solar Cell Through Triple-Graded Approach," *Journal of Electronic Materials*, 50, no. 12, pp. 6756-6765.
5. Cha, M., Da, P., Wang, J., Wang, W., Chen, Z., Xiu, F., Zheng, G., & Z.-S. J. J. o. t. A.C. S. Wang (2016). "Enhancing perovskite solar cell performance by interface engineering using CH<sub>3</sub>NH<sub>3</sub>PbBr<sub>0.9</sub>I<sub>0.1</sub> quantum dots," 138, no. 27, pp. 8581-8587.
6. Bhattacharai, S., Hossain, I., Maiti, M., Pandey, R., & Madan, J. (2023). "Performance analysis and optimization of all-inorganic CsPbI<sub>3</sub>-based perovskite solar cell," *Indian Journal of Physics*, 2023.
7. Lakhdar, N., & Hima, A. (2020). "Electron transport material effect on performance of perovskite solar cells based on CH<sub>3</sub>NH<sub>3</sub>GeI<sub>3</sub>," *Optical Materials*, 99, pp. 109517.
8. Pandey, R., Madan, J., & Sharma, R. (2021). "Enhanced Charge Extraction in Metal- Perovskite-Metal Back-Contact Solar Cell Structure Through Electrostatic Doping: A Numerical Study," *IEEE Transactions on Electron Devices*, PP, pp. 1-7.
9. Raoui, Y., Ez-Zahraouy, H., Kazim, S., & Ahmad, S. (2021). "Energy level engineering of charge selective contact and halide perovskite by modulating band offset: Mechanistic insights," *Journal of Energy Chemistry*, 54, pp. 822-829.
10. Rahman, M. S., Miah, S., Marma, M. S. W., & Ibrahim, M. (n.a). "Numerical Simulation of CsSnI<sub>3</sub>-based Perovskite Solar Cells: Influence of doped-ITO Front Contact." pp. 140- 145.
11. Bhattacharai, S., Sharma, A., & Das, T. D. (2020). "Efficiency enhancement of perovskite solar cell by using doubly carrier transport layers with a distinct bandgap of MAPbI<sub>3</sub> active layer," *Optik*, 224, pp. 165430.
12. Ahmed, S., Karim, M. Rahman, A., M. H., Aktar, A., Islam, M. R., Islam, A., & Bakar Md. Ismail, A. (2021). "Performance analysis of lead-free CsBi<sub>3</sub>I<sub>10</sub>-based perovskite solar cell through the numerical calculation," *Solar Energy*, 226, pp. 54-63.
13. Bhattacharai, S., Mhamdi, A., Hossain, I., Raoui, Y., Pandey, R., Madan, J., Bouazizi, A., Maiti, M., Gogoi, D., & Sharma A. (2022). "A detailed review of perovskite solar cells: Introduction, working principle, modelling, fabrication techniques, future challenges," *Micro and Nanostructures*, 172, pp. 207450.
14. Kojima, A., Teshima, K., Shirai, Y., & Miyasaka, T. (2009). "Organometal Halide Perovskites as Visible-Light Sensitizers for Photovoltaic Cells," *Journal of the*

- American Chemical Society*, 131, no. 17, pp. 6050-6051.
15. Kim, H.-S., Seo, J.-Y., & Park, N.-G. (2016). "Material and Device Stability in Perovskite Solar Cells," *ChemSusChem*, 9, no. 18, pp. 2528-2540.
  16. Bhattarai, S., Sharma, A., & Das T. D. (2020). "Factor affecting the performance of perovskite solar cell for distinct MAPI layer thickness," *AIP Conference Proceedings*, 2269, no. 1, pp. 030071.
  17. Bhattarai, S., & Das, T. D. (2021). "Optimization of the perovskite solar cell design to achieve a highly improved efficiency," *Optical Materials*, 111, pp. 110661.
  18. Bhattarai, S., Sharma, A., Muchahary, D., Gogoi, D., & Das, T. D. (2021). "Numerical simulation study for efficiency enhancement of doubly graded perovskite solar cell," *Optical Materials*, 118, pp. 111285.
  19. Bhattarai, S., Pandey, R., Madan, J., Muchahary, D., & Gogoi, D. (2022). "A novel graded approach for improving the efficiency of Lead-Free perovskite solar cells," *Solar Energy*, vol. 244, pp. 255-263.
  20. Madan, J., Garg, S., Gupta, K., Rana, S., Manocha, A., & Pandey, R. (2020). "Numerical simulation of charge transport layer free perovskite solar cell using metal work function shifted contacts," *Optik*, 202, pp. 163646.
  21. Bhattarai, S., & Das, T. D. (2021). "Optimization of carrier transport materials for the performance enhancement of the MAGeI3 based perovskite solar cell," *Solar Energy*, 217, pp. 200-207.
  22. Karthick, S., Velumani, S., & Bouclé, J. J. S. E. (2020). "Experimental and SCAPS simulated formamidinium perovskite solar cells: a comparison of device performance," 205, pp. 349-357.
  23. Adhikari, N., Dubey, A., Gaml, E. A., Vaagensmith, B., Reza, K. M., Mabrouk, S. A. A., Gu, S., Zai, J., Qian, X., & Qiao, Q. J. N. (2016). "Crystallization of a perovskite film for higher performance solar cells by controlling water concentration in methyl ammonium iodide precursor solution," 8, no. 5, pp. 2693-2703.
  24. Rai, S., Pandey, B. K., & Dwivedi, D. K. (2020). "Modeling of highly efficient and low cost CH<sub>3</sub>NH<sub>3</sub>Pb (I<sub>1-x</sub>Cl<sub>x</sub>)<sub>3</sub> based perovskite solar cell by numerical simulation," *Optical Materials*, 100, pp. 109631.

**Copyright:** ©2023 Sagar Bhattarai. This is an open-access article distributed under the terms of the Creative Commons Attribution License, which permits unrestricted use, distribution, and reproduction in any medium, provided the original author and source are credited.